Arch. Mech., **70**, 1, pp. 89–102, Warszawa 2018
SEVENTY YEARS OF THE ARCHIVES OF MECHANICS

Double-diffusive convection in an anisotropic porous layer using the Darcy–Brinkman–Forchheimer formulation

S. SAFI[1], S. BENISSAAD[2]

[1] *Laboratoire d'Énergétique Appliqué et de Pollution*
Faculté des Sciences de la Technologie
Université des Frères Mentouri
Constantine 1, Algeria
e-mail: safia.safi@umc.edu.dz

[2] *Laboratoire d'Énergétique Appliqué et de Pollution*
Départament de Génie Mécanique
Faculté des Sciences de la Technologie
Université des Frères Mentouri
Constantine 1, Algeria

The aim of this paper is to discuss the double-diffusive natural convection in an anisotropic porous medium saturated with a binary fluid. The vertical walls of porous cavity are subjected to uniform temperature and concentration whereas the other surfaces are assumed to be adiabatic and impermeable. Darcy–Brinkman–Forchheimer model with the Boussinesq approximation was used to formulate the problem and the finite volume method was adopted to resolve the governing equations system. A parametric study was conducted and the results are presented and analyzed. They showed an excellent agreement in comparison with those reported in literature. They also allowed the evaluation of the control parameters effect on the flow structure, heat and mass transfer.

Key words: natural convection, anisotropic porous media, Darcy–Brinkman–Forchheimer.

1. Introduction

The combined heat and mass transfer in saturated porous media continues to interest many researchers because of its use in several engineering fields.

Ingham and Pop (eds.) [1], Nield and Bejan [2] and Vafai (ed.) [3] have, respectively, reported in their books, a review of the literature concerning the determination of convective heat and mass transfer in saturated porous media.

Natural convection in anisotropic porous media has received relatively little attention despite its large range of applications. The work concerns such a problem undertaken by Ni and Beckermann [4] who studied the natural convection flow and heat transfer in a vertical enclosure filled with homogeneous, hydrodynamically and thermally porous anisotropic media. Their results showed an enhancement of the Nusselt number by a large permeability ratio and its reduction by a low one. A large thermal conductivity ratio, also, caused a smaller Nusselt number and a low thermal conductivity ratio has an insignificant effect on the heat transfer pattern. Bera *et al.* [5] conducted a study on thermosolutal convection within a rectangular enclosure. They observed significant changes in the Nusselt and Sherwood numbers caused by the anisotropy and a maximum of mass transfer was obtained for a critical thermal anisotropy ratio. Baytas and Pop [6] carried out a numerical analysis for the steady-state free convection within an inclined cavity filled with a fluid-saturated porous medium. The cavity walls were kept at a constant temperature while the horizontal walls were insulated. Their results concerned momentum and heat transport characteristics within the Rayleigh number, enclosure aspect ratio and inclined angle. Ress and Postelnicu [7] analysed the onset of convection in an inclined porous anisotropic layer in both permeability and thermal diffusivity, heated from below. It has been observed that the transition between longitudinal and transverse rolls was often smooth rather than abrupt when the governing parameters are varied. Bennacer *et al.* [8] studied double-diffusive natural convection in a vertical cavity filled with a saturated anisotropic porous medium. The medium was assumed to be hydrodynamically anisotropic with the principal axes of anisotropic permeability. The cavity side walls were maintained at constant temperatures and concentrations, while the horizontal walls were adiabatic and impermeable. The results indicated the existence of three regimes: a diffusive regime for low values of anisotropy (K), a transition regime when Nusselt and Sherwood numbers increased for larger value of K and an asymptotic regime where Nusselt and Sherwood numbers became independent of K. The transition between the different regimes depends on the thermal Rayleigh number, buoyancy ratio and the Lewis number. Hadad [9] studied the effect of anisotropy and the variable permiability in a vertical direction for the problem of convection in a Darcy porous medium. Linear instability results proved that the nonlinear energy stability bound was the same as the linear one. Singh and al. [10] studied heatlines for natural convection heat transfer inclined porous square cavities. The obtained results showed that the larger inclination angle may be optimal for the energy efficient processes involving inclined enclosures due to larger heat flow circulations with enhanced thermal mixing.

The problem of double-diffusive convection in an inclined horizontal bilayered porous cavity was considered by [11]. The numerical results were presented and analyzed in terms of streamlines, isotherms, isoconcentrations lines and average Nusselt and Sherwood numbers. Numerical and a scale analysis were used to characterize the effect of the permeability ratio on the heat and mass transfer in vertical bi-layered porous cavity. HARFASH and HILL [12] simulated a three dimensional double-diffusive through flow in an internally heated anisotropic porous media. The linear threshold could accurately predict the onset of instability in the steady state through flow.

The aim of the present study is to emphasize how the natural convection and heat and mass transfer in an anisotropic porous layer. The saturated porous medium is anisotropic in permeability and thermal conductivity. The orientations of the permeabilities K_x and K_y are inclined with respect to a coordinate system by an angle α. To study such a problem, a rectangular cavity with the aspect ratio $A = 4$ is used. The formulation is based on the Darcy–Brinckman–Forchheimer model and the thermosolutal convection is studied. Effects of many parameters such as the inclination angle and permeability ratio on particularly heat and mass transfer are discussed.

2. Problem formulation

Figure 1 presents the studied physical model. It is represented by a horizontal porous layer, with the aspect ratio $(A = L/H) = 4$, saturated by a binary fluid. The porous medium was considered homogeneous and anisotropic in permeability and thermal conductivity. Directions of equivalent thermal conductivities λ_1, λ_2 coincide respectively with the horizontal and vertical axes. The permeabilities are denoted by K_1 and K_2. They make an angle α with the principal axes of the cavity. The anisotropy ratio is then defined as $K^* = K_2/K_1$. The vertical walls of the porous cavity were subjected to uniform conditions of temperature and concentration whereas the horizontal walls are assumed to be adiabatic and impermeable. A general model of Darcy–Brinkman–Forchheimer was used to account for the flow in the porous medium.

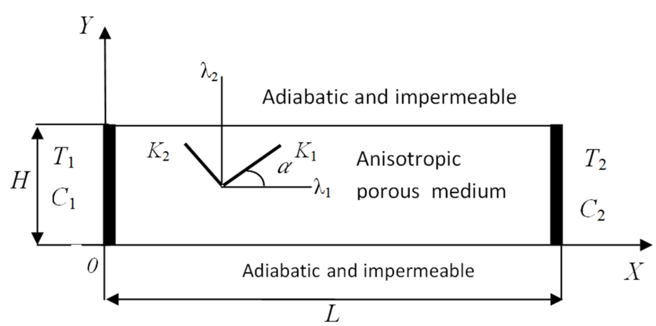

FIG. 1. Physical situation and coordinate system.

Under the usual Boussinesq approximation, the governing equations for steady two-dimensional natural convection flow in the porous cavity using conservation of mass, momentum, energy and species are expressed as:

Continuity equation

$$\nabla \cdot V' = \frac{\partial u'}{\partial x'} + \frac{\partial v'}{\partial y'} = 0. \tag{2.1}$$

Momentum equation

$$\rho_f \left[\frac{1}{\varphi} \frac{\partial V'}{\partial t'} + \frac{1}{\varphi^2} (V' \cdot \nabla) V' \right] = -\nabla P' - \mu \frac{V'}{\overline{\overline{K}}''} - \frac{C_f}{\overline{\overline{K}}''^{1/2}} V' |V'| + \mu_{eff} \nabla^2 V' + \rho_f \vec{g}. \tag{2.2}$$

Energy equation

$$\sigma \frac{\partial T'}{\partial t'} + V' \cdot \nabla T' = \nabla \cdot (\overline{\overline{\Lambda}} \nabla T'). \tag{2.3}$$

Concentration equation

$$\varphi \frac{\partial C'}{\partial t'} + V' \cdot \nabla C' = \nabla \cdot (D_{eq} \nabla C'). \tag{2.4}$$

Where: $|V'|$ denotes the magnitude of velocity vector $(\sqrt{u'^2 + v'^2})$; u' and v' are dimensional horizontal and vertical velocities; x' and $'y$ are dimensional horizontal and vertical coordinates and T', C', P' and t' are the dimensional, temperature, concentration, pressure and time, respectively; ρ_f is the fluid density; g is the gravity acceleration; μ is dynamic viscosity of the fluid; μ_{eff} is the apparent dynamic viscosity for Brinkman's model; D_{eq} is the equivalent mass diffusivity; φ is the porosity; C_f is the Forchheimer coefficient; σ is the ratio of heat capacities $= (\rho c)_m / (\rho c)_f$; with $(\rho c)_f$ is the thermal heat capacity of the fluid and $(\rho c)_m$ is the thermal heat capacity of the saturated porous medium.

$\overline{\overline{K}}''$ and $\overline{\overline{\Lambda}}$ are the second order flow permeability and thermal conductivity tensors of the saturated porous medium

$$\overline{\overline{K}}'' = \begin{bmatrix} K_1(\cos\alpha)^2 + K_2(\sin\alpha)^2 & (K_1 - K_2)\sin\alpha\cos\alpha \\ (K_2 - K_1)\sin\alpha\cos\alpha & K_1(\sin\alpha)^2 + K_2(\cos\alpha)^2 \end{bmatrix}. \tag{2.5}$$

The permeability tensor may be expressed as $\overline{\overline{K}}'' = K_2 \overline{\overline{K}}$, in which

$$\overline{\overline{K}} = \begin{bmatrix} \frac{1}{K^*}(\cos\alpha)^2 + (\sin\alpha)^2 & \left(\frac{1}{K^*} - 1\right)\sin\alpha\cos\alpha \\ \left(\frac{1}{K^*} - 1\right)\sin\alpha\cos\alpha & \frac{1}{K^*}(\cos\alpha)^2 + (\sin\alpha)^2 \end{bmatrix} \tag{2.6}$$

is a dimensionless form of the permeability tensor.

The inverse of $\overline{\overline{K}}$ is defined as:

$$\overline{\overline{K}}^{-1} = \begin{bmatrix} K^*(\cos\alpha)^2 + (\sin\alpha)^2 & (K^*-1)\sin\alpha\cos\alpha \\ (K^*-1)\sin\alpha\cos\alpha & K^*(\cos\alpha)^2 + (\sin\alpha)^2 \end{bmatrix}. \tag{2.7}$$

The thermal conductivity tensor may be expressed as:

$$\overline{\overline{\Lambda}} = \begin{bmatrix} \lambda_1 & 0 \\ 0 & \lambda_2 \end{bmatrix}. \tag{2.8}$$

The inverse of $\overline{\overline{\Lambda}}$ is defined as:

$$\overline{\overline{\Lambda}}^{-1} = \begin{bmatrix} \lambda & 0 \\ 0 & 1 \end{bmatrix}. \tag{2.9}$$

with $\lambda = \lambda_2/\lambda_1$.

The dimensionless governing equations are written as:

$$\frac{\partial U}{\partial X} + \frac{\partial V}{\partial Y} = 0, \tag{2.10}$$

$$\begin{aligned} &\frac{1}{\varphi}\frac{\partial U}{\partial \tau} + \frac{1}{\varphi^2}\left(U\frac{\partial U}{\partial X} + V\frac{\partial U}{\partial Y}\right) \\ &= -\frac{\partial P}{\partial X} + \frac{Pr}{\varphi}\left(\frac{\partial^2 U}{\partial X^2} + \frac{\partial^2 U}{\partial Y^2}\right) - \frac{Pr}{D\alpha}\Big[U(K^*(\cos\alpha)^2 + (\sin\alpha)^2) \\ &\quad + V((K^*-1)\sin\alpha\cos\alpha) - \frac{C_f}{\sqrt{D\alpha}}[U(\sqrt{K^*}(\cos\alpha)^2 + (\sin\alpha)^2)] \\ &\quad + V((\sqrt{K^*}-1)\sin\alpha\cos\alpha)\Big]\sqrt{U^2+V^2}. \end{aligned} \tag{2.11}$$

$$\begin{aligned} &\frac{1}{\varphi}\frac{\partial V}{\partial \tau} + \frac{1}{\varphi^2}\left(U\frac{\partial V}{\partial X} + V\frac{\partial V}{\partial Y}\right) \\ &= -\frac{\partial P}{\partial Y} + \frac{Pr}{\varphi}\left(\frac{\partial^2 V}{\partial X^2} + \frac{\partial^2 V}{\partial Y^2}\right) - \frac{Pr}{D\alpha}[U((K^*-1)(\sin\alpha\cos\alpha)^2) \\ &\quad + V(K^*(\cos\alpha)^2 + (\sin\alpha)^2] - \frac{C_f}{\sqrt{D\alpha}}[U((1-\sqrt{K^*})\sin\alpha + \cos\alpha) \\ &\quad + V(\sqrt{K^*}(\cos\alpha)^2 + (\sin\alpha)^2]\sqrt{U^2+V^2} + PrRa(T+NC), \end{aligned} \tag{2.12}$$

$$\frac{\partial T}{\partial \tau} + \left(U\frac{\partial T}{\partial X} + V\frac{\partial T}{\partial Y}\right) = \frac{1}{Pr}\overline{\overline{\Lambda}}^{-1}\left(\frac{\partial^2 T}{\partial X^2} + \frac{\partial^2 T}{\partial Y^2}\right), \tag{2.13}$$

$$\frac{\partial C}{\partial \tau} + \frac{1}{\varphi}\left(U\frac{\partial C}{\partial X} + V\frac{\partial C}{\partial Y}\right) = \frac{1}{Le}\left(\frac{\partial^2 C}{\partial X^2} + \frac{\partial^2 C}{\partial Y^2}\right), \tag{2.14}$$

where (X, Y) are the dimensionless horizontal and vertical coordinate and (U, V) are dimensionless velocity in (X, Y) direction; τ, P, T and C are respectively the dimensionless time, pressure, temperature and concentration

$$
(2.15)\qquad \begin{cases} (X,Y)=\left(\dfrac{x'}{H'},\dfrac{y'}{H}\right), & (U,V)=\left(\dfrac{u'H}{a},\dfrac{v'H}{a}\right),\\ P=\dfrac{p'H^2}{\rho_f a^2}, & \tau=\dfrac{t'}{\sigma a},\\ C=\dfrac{(C'-C'_m)}{\Delta C'}, & T=\dfrac{(T'-T'_m)}{\Delta T'}, \end{cases}
$$

where H and L are the height and the length of the cavity, respectively, a is the thermal diffusivity of a porous medium, $\Delta C'$ is the characteristic concentration difference $= C'_1 - C'_2$, $\Delta T'$ is the characteristic temperature difference $= T'_1 - T'_2$, C_m is the reference solute concentration $= (C'_1 + C'_2)/2$, $T'_m$is the reference temperature $= (T'_1 + T'_2)/2$.

The non-dimensional boundary conditions associated to this problem are as follows:

$$(2.16)\qquad U=V=0,\quad T=0 \text{ and } C=0 \text{ at } \tau=0,$$

$$(2.17)\qquad \frac{\partial T}{\partial Y}=0,\quad \frac{\partial C}{\partial Y}=0,\quad U=V=0 \text{ at } Y=0,\ \forall X,$$

$$(2.18)\qquad \frac{\partial T}{\partial Y}=0,\quad \frac{\partial C}{\partial Y}=0,\quad U=V=0 \text{ at } Y=1,\ \forall X,$$

$$(2.19)\qquad T=1,\quad C=0,\quad U=V=0 \text{ at } X=0,\ \forall Y,$$

$$(2.20)\qquad T=0,\quad C=1,\quad U=V=0 \text{ at } X=L/H,\ \forall Y,$$

The dimensionless variables are defined as: Darcy number ($Da = K_2/H^2$), Prandtl number ($Pr = v/a$), Rayleigh number ($Ra = g\beta_T \Delta T H^3/(av)$), Lewis number ($Le = a/D$) and Buoyancy ratio number ($N = \beta_S \Delta C/(\beta_T \Delta T)$), where β_S and β_T are respectively coefficient of volumetric solutal and thermal expansion, ΔT and ΔC are respectively the temperature and concentration differences. is the kinematic viscosity.

The average Nusselt and Sherwood numbers are defined by

$$(2.21)\qquad Nu=\int_0^1\left(\frac{\partial T}{\partial X}\right)_{X=0} dY,$$

$$(2.22)\qquad Sh=\int_0^1\left(\frac{\partial C}{\partial X}\right)_{X=0} dY.$$

3. Numerical method

The governing equations (2.10) to (2.14) with the boundary conditions and initial conditions were discretized by the finite volume method on an irregular staggered grid system using the SIMPLER algorithm of PATANKAR [13]. A refined mesh has been employed near the walls. The velocity components were stored on the faces of control volumes and other variables pressure and temperature were stored at the nodes of the staggered mesh. Finally, the discretized algebraic equations were solved iteratively by the line-by-line using the TDMA algorithm adapted to a tri-diagonal matrix system.

However, the discretized momentum, energy and concentration equations include transient terms; so, the pseudo-transient strategy will be used. This consists of calculations from a given initial field by means of a pseudo-transient computation starting from the same initial field by taking a step size at each time level until convergence is achieved. Alternatively steady state calculations may be interpreted as pseudo-transient solutions with spatially varying time steps VERSTEEG and MALALASEKERA [14].

Convergence to a steady state is reached when the mass and energy balance is satisfied after each iteration by checking that the relative difference of the dependent variable between two successive iterations is less than a user defined accuracy criterion given by

$$\left(\left|\frac{\phi_{i,j}^{t+\Delta t}-\phi_{i,j}^{t}}{\phi_{i,j}^{t+\Delta t}}\right|\right)\leq 10^{-4}, \tag{2.23}$$

where ϕ corresponds to U, V, T and C. The indices i, j indicate a mesh point. Δt is the time increment.

Many sized grids were used to obtain satisfactory solutions. Figures 2 and 3 illustrate, respectively, the distribution of the horizontal u – velocity in the vertical mid plane ($X = L/2$) and the temperature at the horizontal mid plane

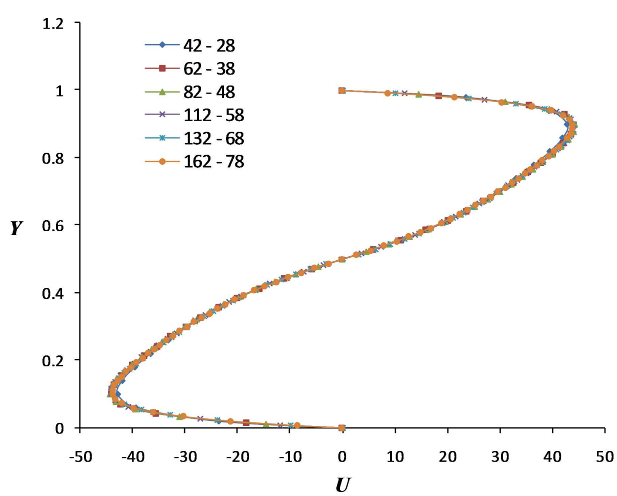

FIG. 2. Horizontal velocity profiles (u) in the vertical mid plane, $X = L/2$ ($Da = 10^{-3}$, $N = 0$, $Ra = 10^6$, and $\alpha = 0°$).

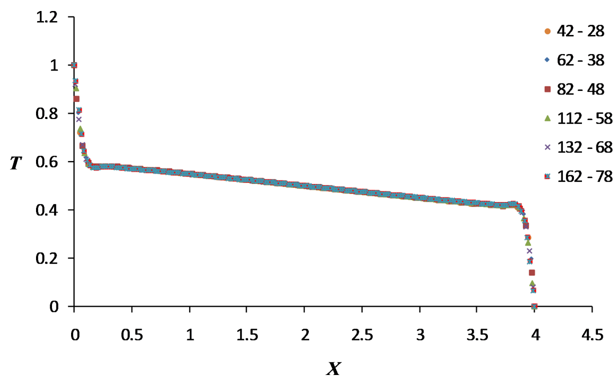

FIG. 3. Temperature profiles in the horizontal mid plane, $Y = L/2$ ($Da = 10^{-3}$, $N = 0$, $Ra = 10^6$, and $\alpha = 0°$).

($Y = H/2$). It is observed that the curves of velocities and the temperatures overlap with each other for all grids. So a grid number of 132×68 was chosen for all computations.

For the accuracy of the results, the present study was compared with those reported in literature. Typical results are presented in Tables 1–3 for, respectively, the case of isotropic and anisotropic porous media.

Tables 1 and 2 show the results for the thermal convection in an isotropic porous medium, respectively, for Darcy regime and Darcy–Brinkman regime.

Table 1. Comparison of the Nusselt number in the case of the Darcy regime, in thermal convection ($Da = 10^{-7}$, $A = 1$, $Pr = 0.71$, $N = 0$.

$Ra^* = Ra.\ Da$	LAURIAT and PRASSAD [15]	TREVESION and BEJAN [16]	NITHIARASU *et al.* [17]	YOUNSI *et al.* [18]	Present study
10	1.07	/	1.08	1.06	1.078
50	/	2.02	1.958	1.936	1.976
100	3.09	3.27	3.02	2.98	3.089
500	/	/	8.38	8.32	8.69
1000	13.41	18.38	12.514	12.32	12.7

Table 2. Comparison of the Nusselt number in the case of the Darcy–Brinkman regime, in thermal convection ($A = 1$, $Pr = 0.71$).

	Da	Nu					
		10^{-8}	10^{-6}	10^{-5}	10^{-4}	10^{-3}	10^{-2}
Present study	$Ra^* = 500$	8.83	8.81	8.63	7.61	5.46	3.26
BENNACER *et al.* [19]		8.80	8.68	8.37	7.30	5.38	3.26
LAURIAT and PRASSAD [20]		8.84	8.72	8.41	7.35	5.42	3.30
Present study	$Ra^* = 10^3$	13.09	–	12.73	–	–	4.19
BENNACER *et al.* [19]		13.48	–	12.26	–	–	4.18
LAURIAT and PRASSAD [20]		13.41	–	12.42	–	–	4.26

From this comparison, it can be noticed that the maximal difference between these results remains less than 3%.

Table 3 presents the results for an anisotropic porous medium. The maximal difference between these results does not exceed 1.5%.

Table 3. Comparison of the Nusselt numbers in anisotropic porous medium ($\boldsymbol{Da} = 10^{-7}$, $A = 1$, $\boldsymbol{Ra} = 10^3$, $N = 0$, $\alpha = 0°$).

$K^* = K_2/K_1$	10^3	10^2	10^1	10^0	10^{-1}	10^{-2}
NI and BECKERMANN [4]	1.01	1.30	4.17	13.41	37.37	80.34
BENNACER *et al.* [8]	1.00	1.29	4.17	13.48	37.56	80.62
Present study	1.04	1.26	4.19	13.09	37.31	80.33

The results presented above, showed a good accuracy and then were satisfactory.

4. Results and discussion

The present results have been obtained for wide ranges of parameters. The inclination angle α varied from 0° to 60°, the anisotropic permeability ratio K^* varied within 10^{-4} to 10^3 and the thermal conductivity λ varied from 10^{-3} to 10^3. The Prandtl number and the Forchheimer constant were set to be respectively 0.71 and 0.55. The Rayleigh number varied from 10^6 to 10^8 for the different buoyancy ratio N.

4.1. Study of flow structure, temperature and concentration fields

Figures 4–6 display streamlines, isotherms and isoconcentrations for the Rayleigh number ($Ra = 10^6$) and the Darcy number ($Da = 10^{-3}$), with inclination angles, $\alpha = 0°$; 30° and 60° for various K^* varying within 0.1 to 10.

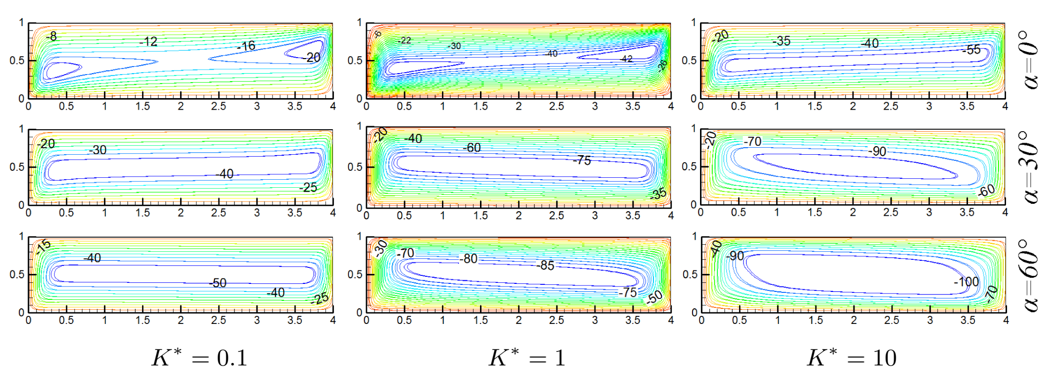

FIG. 4. Streamlines for various values of K^* and α ($Da = 10^{-3}$, $N = 0$, $Ra = 10^4$, $\lambda = 10.$)

It is readily seen from Fig. 4 that for $K^* = 10$, the flow pattern is channelled along the thermally active vertical walls, while it is strongly channelled along the horizontal boundaries for $\alpha = 0°$ and $K^* = 10^{-1}$. This is due to the relatively high permeability in that direction. However, as α increases to 30° and 60°, the fluid motion is represented by one clockwise vortex inside the cavity and the intensity of the flow is very weak as observed from stream function contours.

Figure 5 illustrates the isotherms contours for $\alpha = 0°$, 30° and 60°, respectively. They are more distorted from left to right. This reflects the intensification of the convection. The thermal boundary layer is developed in the upper part of the cavity walls.

The effect of various inclination angles α for $K^* = 0.1$ to 10 on isoconcentrations are shown in Fig. 6. The isoconcentrations increase as the anisotropic permeability ratio K^* increase. They are confined near the active walls of the cavity. However, a further increase of K^* for any angle of inclination α significantly changes the concentration field.

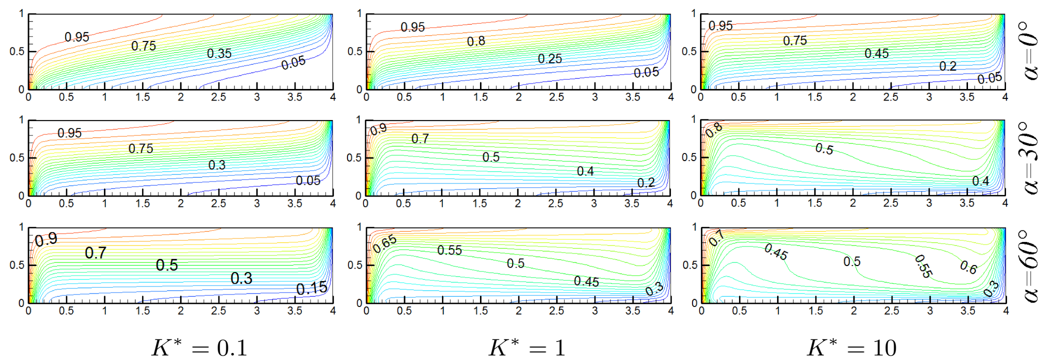

Fig. 5. Isotherms for various values of K^* and α ($Da = 10^{-3}$, $N = 0$, $Ra = 10^4$, $\lambda = 10$.)

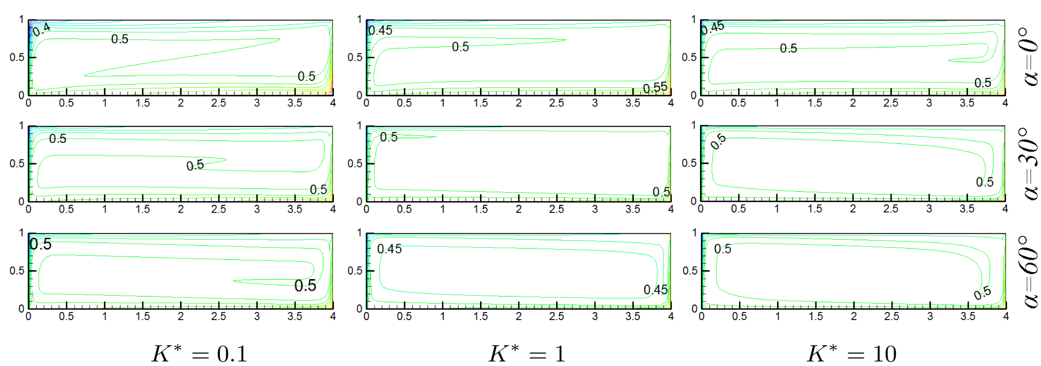

Fig. 6. Isoconcentrations for various values of K* and α ($Da = 10^{-3}$, $N = 0$, $Ra = 10^4$, $\lambda = 10$.)

4.2. Nusselt and Sherwood numbers

The average Nusselt and Sherwood numbers with different permeability ratios K^*at various inclinations of principal axes α ($\alpha = 0°$, $30°$ and $60°$) are shown in Fig. 7a and 7b. Different values of the Rayleigh number ($Ra = 10^6$ and 10^8), $Da = 10^{-3}$, and $\lambda = 10$ are taken into consideration. We notice a continuous transition for Nusselt and Sherwood from its minimum to its maximum values, with increasingK^*. Three stages are observed in theses curves. The first one is characterized by low values of Nu and Sh. As the permeability ratio K^* increases from 10^{-3} to 10, the heat and mass transfer increase sharply. That is the second one. For further grow up of the permeability ratio, the heat and mass transfer remain almost constant. That is the third stage. In each of these cases, the Sherwood number is greater than the Nusselt number. An optimal inclination value for which the heat and mass transfers are maximal exists. For the parameters used ($Le = 10$, $N = 10$, $Da = 10^{-3}$, $\lambda = 10$) the optimal angle is equal to $30°$, also the heat and mass transfer decrease when the angle of inclination is equal to $60°$.

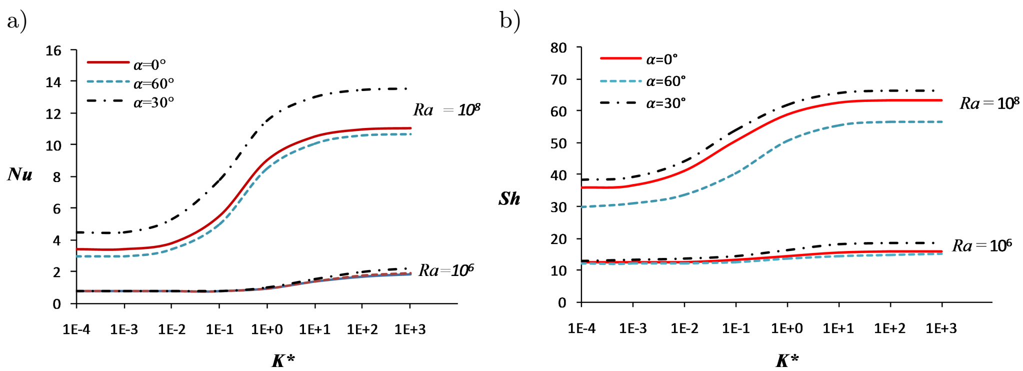

FIG. 7. a) Effect of K^* on heat transfer and b) mass transfer for various values of Ra and α ($Da = 10^{-3}$, $\lambda = 10$ and $N = 0$).

Figures 8a and 8b illustrate the effect of buoyancy ratio N on heat and mass transfer with different angles of inclination α. The minimum Nusselt and Sherwood numbers go up with the increase of buoyancy ratio N. For a fixed value of N, the heat and mass transfers increase with the increase of the anisotropy permeability ratio. Three stages are then noticed. The first stage is characterized by a slow increase of Nu and Sh. The second one is characterized by an important increase of Nu and Sh numbers. It corresponds to the anisotropy permeability ratio K^* from 10^{-2} until 10. After that, they were almost constant. The highest values of Nusselt and Sherwood numbers occur at about $30°$. They are smaller for the inclination angle equal to $60°$.

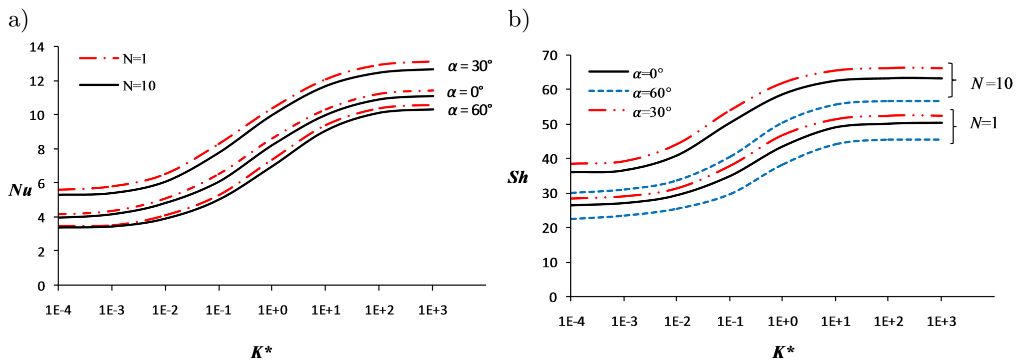

Fig. 8. Effect of K^* on a) heat transfer and b) mass transfer for various values of N ($Da = 10^{-3}$, $\lambda = 10$ and $Ra = 10^4$).

The influence of the thermal conductivity ratio λ on heat and mass transfer is depicted in Figs. 9a and 9b. These curves are obtained for fixed values of anisotropy permeability ratio K^* ($K^* = 10^{-1}$, 1 and 10) and the enclosure inclination angle $\alpha = 0°$. It is seen from these curves that Nusselt augments almost linearly with the increasing value of λ. Such increases are greater with a greater value of K^*. However, two distinctive stages are observed in the case of Sherwood number: an increasing stage and a decreasing one. The increase in λ induces an increase in the number of Sherwood until reaching a maximum for a λ value corresponding to 10. Beyond this value, the mass transfer decreases. For fixed K^* and for the thermal anisotropy ratio λ becoming weakest, the Sherwood number tends towards diffusive transfers. It is also worth noting that the Nusselt and Sherwood numbers are greater for a lower Darcy number.

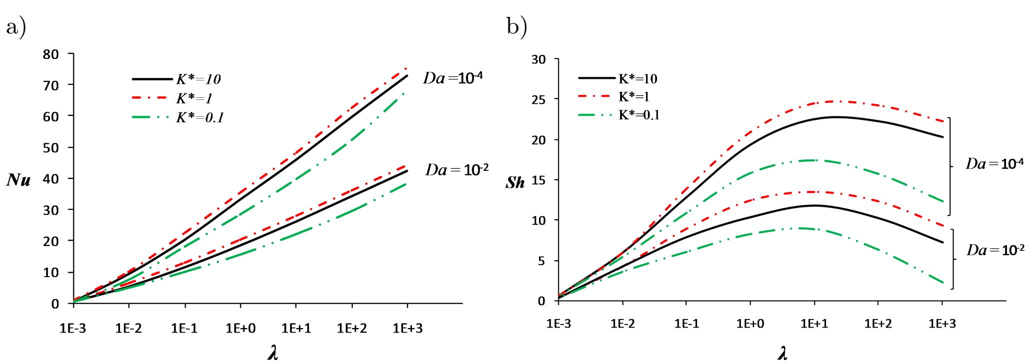

Fig. 9. Effect of thermal anisotropy ratio λ on a) heat transfer and b) mass transfer ($Ra = 10^4$, $N = 0$ and various values of K^* and Da).

5. Conclusions

A numerical simulation of the natural convection in a horizontal porous cavity saturated by a binary fluid was carried out. The porous medium was assumed to be anisotropic in both permeability and thermal conductivity. The focus of the work was on the validity of the Darcy–Brinkman Forchheimer model when various combinations of the thermal Rayleigh number, inclination angle, permeability ratio, thermal conductivity and buoyancy ratio were considered. Results are analyzed and discussed according to the study parameters. Their comparison with those available in the literature showed good agreement. It was observed that the different parameters have strong effects on heat and mass transfer as well as fluid flow. The heat and mass transfer rates increased with the increasing of the permeability ratio. Inclination angle effect on the heat and mass transfer was clearly observed. It was also observed that the Nusselt and Sherwood numbers increase with the increase of the buoyancy ratio and thermal Rayleigh number.

References

1. D. B. Ingham, I. Pop, *Transport Phenomena in Porous Media*, Pergamon Press, New York, 1998.
2. D.A. Nield, A. Bejan, *Convection in Porous Media*, Springer, New York, 2013.
3. K. Vafai, *Handbook of Porous Media*, Taylor/CRC Press, Francis, London/Boca Raton, FL, 2005.
4. J. Ni, C. Beckermann, *Natural convection in a vertical enclosure filled with anisotropic porous media*, Journal of Heat Transfer, **113**, 1033–1037, 1991.
5. P. Bera, V. Eswaran, P. Singh, *Numerical study of heat and mass transfer in an anisotropic porous enclosure due to constant heating and cooling*, Numerical Heat Transfer, **34**, 887–905, 1998.
6. A.C. Baytas, I. Pop, *Free convection in oblique enclosures filled with a porous medium*, International Journal of Heat and Mass Transfer, **42**, 1047–1057, 1999.
7. D.A.S. Rees, A. Postelnicu, *The onset of convection in an inclined anisotropic porous layer*, International Journal of Heat and Mass Transfer, **44**, 4127–4138, 2001.
8. R. Bennacer, A. Tobbal, H. Beji, *Double diffusive convection in a vertical enclosure filled with anisotropic porous media*, International Journal of Thermal Sciences, **40**, 30–41, 2001.
9. S.A.M. Haddad, Thermal convection in a darcy porous medium with anisotropic spatially varying permeability, Acta Applicandae Mathematicae, **132**, 359–370, 2014.
10. A.K. Singh, T. Basak, A. Nag, S. Roy, *Heatlines and thermal management analysis for natural convection within inclined porous square cavities*, International Journal of Heat and Mass Transfer, **8**, 583–597, 2015.

11. N. Hadidi, R. Bennacer, Y. Ould-Amer, *Two-dimensional thermosolutal natural convective heat and mass transfer in a bi-layered and inclined porous enclosure*, Energy, **93**, 2582–2592 , 2015.

12. A.J. Harfash, A.A. Hill, *Simulation of three dimensional double-diffusive through flow in internally heated anisotropic porous media*, International Journal of Heat and Mass Transfer, **72**, 609–615, 2014.

13. S.V. Patankar, *Numerical Heat Transfer and Fluid Flow*, Hemisphere, New York, 1980.

14. H.K. Versteeg, W. Malalasekera, *An Introduction to Computational Fluid Dynamics. The Finite Volume Method*, 2nd ed., Pearson Education Limited, Glasgow, 262–266, 2007.

15. G. Lauriat, V. Prassad, *Non-Darcian effect on natural convection in a vertical porous enclosure*, International Journal of Heat and Mass Transfer, **32**, 11, 2135–2148, 1989.

16. O.V. Trevisan, A. Bejan, *Natural convection with combined heat and mass transfer buoyancy effects in a porous medium*, International Journal of Heat and Mass Transfer, **28**, 1597–1611, 1985.

17. P. Nithiarasu, K. N. Seetharamu, T. Sundararajan, *Double-diffusive natural convection in an enclosure filled with fluid-saturated porous medium: A generalized non-Darcy approach*, Numerical Heat Transfer, Part A, **30**, 413–426, 1996.

18. R. Younsi, A. Harkati, D. Kalache, *Numerical simulation of double diffusive natural convection in porous cavity: Opposing flow*, Arabian Journal for Science and Engineering, **26**, 2b, 145–155, 2002.

19. R. Bennacer, A. Tobbal, H. Beji, *Natural thermo-solutal convection in porous anisotropic cavity: Darcy-Brinkman formulation*, [in French: Convection naturelle Thermosolutale dans une Cavité Poreuse Anisotrope: Formulation de Darcy–Brinkman], Rev. Energ. Ren., **5**, 1–21, 2002.

20. G. Lauriat, V. Prassad, *Natural convection in vertical porous cavity: Numerical study for Brinkman – extended Darcy formulation*, ASME Journal of Heat Transfer, **109**, 688–696, 1987.

Received September 27, 2017; revised version December 11, 2017.